EUROPEAN ORGANIZATION FOR NUCLEAR RESEARCH

Test of Lepton Flavour Universality in $K^+ \to \ell^+\nu$ Decays

The NA62 collaboration[*]

Abstract

A precision test of lepton flavour universality has been performed by measuring the ratio R_K of kaon leptonic decay rates $K^+ \to e^+\nu$ and $K^+ \to \mu^+\nu$ in a sample of 59813 reconstructed $K^+ \to e^+\nu$ candidates with $(8.71 \pm 0.24)\%$ background contamination. The result $R_K = (2.487 \pm 0.013) \times 10^{-5}$ is in agreement with the Standard Model expectation.

Submitted for publication in Physics Letters B

The NA62 collaboration

C. Lazzeroni, A. Romano

University of Birmingham, Edgbaston, Birmingham, B15 2TT, United Kingdom

A. Ceccucci, H. Danielsson, V. Falaleev, L. Gatignon, S. Goy Lopez [1], B. Hallgren [2], A. Maier, A. Peters, M. Piccini [3], P. Riedler

CERN, CH-1211 Genève 23, Switzerland

M. Dyulendarova, P.L. Frabetti, V. Kekelidze, D. Madigozhin, E. Marinova [3], N. Molokanova, S. Movchan, Yu. Potrebenikov, S. Shkarovskiy, A. Zinchenko

Joint Institute for Nuclear Research, 141980 Dubna (MO), Russia

P. Rubin

George Mason University, Fairfax, VA 22030, USA

W. Baldini, A. Cotta Ramusino, P. Dalpiaz, M. Fiorini [4], A. Gianoli, A. Norton, F. Petrucci, M. Savrié, H. Wahl

Dipartimento di Fisica dell'Università e Sezione dell'INFN di Ferrara, I-44100 Ferrara, Italy

A. Bizzeti [5], F. Bucci [6], E. Iacopini [6], M. Lenti, M. Veltri [7]

Sezione dell'INFN di Firenze, I-50019 Sesto Fiorentino (FI), Italy

A. Antonelli, M. Moulson, M. Raggi, T. Spadaro

Laboratori Nazionali di Frascati, I-00044 Frascati, Italy

K. Eppard, M. Hita-Hochgesand, K. Kleinknecht, B. Renk, R. Wanke, A. Winhart

Institut für Physik, Universität Mainz, D-55099 Mainz, Germany

R. Winston

University of California, Merced, CA 95344, USA

V. Bolotov, V. Duk, E. Gushchin

Institute for Nuclear Research, 117312 Moscow, Russia

F. Ambrosino, D. Di Filippo, P. Massarotti, M. Napolitano, V. Palladino, G. Saracino

Dipartimento di Scienze Fisiche dell'Università e Sezione dell'INFN di Napoli, I-80126 Napoli, Italy

G. Anzivino, E. Imbergamo, R. Piandani, A. Sergi [4]

Dipartimento di Fisica dell'Università e Sezione dell'INFN di Perugia, I-06100 Perugia, Italy

P. Cenci, M. Pepe

Sezione dell'INFN di Perugia, I-06100 Perugia, Italy

F. Costantini, N. Doble, S. Giudici, G. Pierazzini, M. Sozzi, S. Venditti

Dipartimento di Fisica dell'Università e Sezione dell'INFN di Pisa, I-56100 Pisa, Italy

S. Balev [4], G. Collazuol, L. DiLella, S. Gallorini, E. Goudzovski [8,9], G. Lamanna [4], I. Mannelli, G. Ruggiero

Scuola Normale Superiore e Sezione dell'INFN di Pisa, I-56100 Pisa, Italy

C. Cerri, R. Fantechi

Sezione dell'INFN di Pisa, I-56100 Pisa, Italy

V. Kurshetsov, V. Obraztsov, I. Popov, V. Semenov, O. Yushchenko

Institute for High Energy Physics, 142281 Protvino (MO), Russia

G. D'Agostini, E. Leonardi, M. Serra, P. Valente

Sezione dell'INFN di Roma I, I-00185 Roma, Italy

A. Fucci, A. Salamon

Sezione dell'INFN di Roma Tor Vergata, I-00133 Roma, Italy

B. Bloch-Devaux [10], B. Peyaud

DSM/IRFU – CEA Saclay, F-91191 Gif-sur-Yvette, France

J. Engelfried

Instituto de Física, Universidad Autónoma de San Luis Potosí, 78240 San Luis Potosí, Mexico

D. Coward

SLAC National Accelerator Laboratory, Stanford University, Menlo Park, CA 94025, USA

V. Kozhuharov, L. Litov

Faculty of Physics, University of Sofia, 1164 Sofia, Bulgaria

R. Arcidiacono, S. Bifani [11], C. Biino, G. Dellacasa, F. Marchetto

Dipartimento di Fisica Sperimentale dell'Università e Sezione dell'INFN di Torino,
I-10125 Torino, Italy

T. Numao, F. Retiere

TRIUMF, 4004 Wesbrook Mall, Vancouver, British Columbia, V6T 2A3, Canada

---

[1]Present address: CIEMAT, E-28040 Madrid, Spain
[2]Present address: University of Birmingham, Edgbaston, Birmingham, B15 2TT, United Kingdom
[3]Present address: Sezione dell'INFN di Perugia, I-06100 Perugia, Italy
[4]Present address: CERN, CH-1211 Genève 23, Switzerland
[5]Also at Dipartimento di Fisica, Università di Modena e Reggio Emilia, I-41100 Modena, Italy
[6]Also at Dipartimento di Fisica, Università di Firenze, I-50019 Sesto Fiorentino (FI), Italy
[7]Also at Istituto di Fisica, Università di Urbino, I-61029 Urbino, Italy
[8]Present address: CP3, Université catholique de Louvain, B-1348 Louvain-la-Neuve, Belgium
[9]Also at University of Birmingham, Edgbaston, Birmingham, B15 2TT, United Kingdom
[10]Present address: Dipartimento di Fisica Sperimentale dell'Università di Torino, I-10125 Torino, Italy
[11]Present address: University College Dublin School of Physics, Belfield, Dublin 4, Ireland

Introduction

In the Standard Model (SM) the decays of pseudoscalar mesons to light leptons are helicity suppressed. In particular, the SM width of $P^\pm \to \ell^\pm \nu$ decays with $P = \pi, K, D, B$ (denoted $P_{\ell 2}$ in the following) is

$$\Gamma^{\mathrm{SM}}(P^\pm \to \ell^\pm \nu) = \frac{G_F^2 M_P M_\ell^2}{8\pi} \left(1 - \frac{M_\ell^2}{M_P^2}\right)^2 f_P^2 |V_{qq'}|^2, \tag{1}$$

where G_F is the Fermi constant, M_P and M_ℓ are meson and lepton masses, f_P is the decay constant, and $V_{qq'}$ is the corresponding Cabibbo-Kobayashi-Maskawa matrix element. Although the SM predictions for the $P_{\ell 2}$ decay rates are limited by hadronic uncertainties, their specific ratios do not depend on f_P and can be computed very precisely. In particular, the SM prediction for the ratio $R_K = \Gamma(K_{e2})/\Gamma(K_{\mu 2})$ of kaon leptonic decay widths inclusive of internal bremsstrahlung (IB) radiation is [1]

$$R_K^{\mathrm{SM}} = \left(\frac{M_e}{M_\mu}\right)^2 \left(\frac{M_K^2 - M_e^2}{M_K^2 - M_\mu^2}\right)^2 (1 + \delta R_{\mathrm{QED}}) = (2.477 \pm 0.001) \times 10^{-5}, \tag{2}$$

where $\delta R_{\mathrm{QED}} = (-3.79 \pm 0.04)\%$ is an electromagnetic correction due to the IB and structure-dependent effects.

Within the two Higgs doublet models (2HDM), including the minimal supersymmetric model, R_K is sensitive to lepton flavour violating (LFV) effects appearing at the one-loop level via the charged Higgs boson ($H^\pm$) exchange [2, 3], representing a unique probe into mixing in the right-handed slepton sector [4]. The dominant contribution due to the LFV coupling of the $H^\pm$ is

$$R_K^{\mathrm{LFV}} \simeq R_K^{\mathrm{SM}} \left[1 + \left(\frac{M_K}{M_H}\right)^4 \left(\frac{M_\tau}{M_e}\right)^2 |\Delta_R^{31}|^2 \tan^6 \beta\right], \tag{3}$$

where $\tan \beta$ is the ratio of the two Higgs vacuum expectation values, and $|\Delta_R^{31}|$ is the mixing parameter between the superpartners of the right-handed leptons, which can reach $\sim 10^{-3}$. This can enhance R_K by $\mathcal{O}(1\%)$ without contradicting any experimental constraints known at present, including upper bounds on the LFV decays $\tau \to eX$ with $X = \eta, \gamma, \mu\bar{\mu}$.

The first measurements of R_K were performed in the 1970s [5, 6, 7]; the current PDG world average [8] is based on a more precise recent result [9] $R_K = (2.493 \pm 0.031) \times 10^{-5}$. A new measurement of R_K based on a part of the data sample collected by the NA62 experiment at CERN in 2007 is reported in this letter. The analyzed K_{e2} sample is ~ 4 times larger than the total world sample, allowing a measurement of R_K with a precision well below 1%.

1   Beam, detector and data taking

The beam line and setup of the NA48/2 experiment [10, 11] have been used for the NA62 data taking in 2007. Experimental conditions have been optimized for the $K_{e2}/K_{\mu 2}$ measurement.

1.1   Kaon beam

The beam line was originally designed to deliver simultaneous unseparated K^+ and K^- beams derived from the primary 400 GeV/c protons extracted from the CERN SPS. In 2007, the muon sweeping system was optimized for the positive beam, and the sample used for the present analysis was collected with the K^+ beam only. Positively charged particles within a narrow momentum band with a central momentum of 74.0 GeV/c and a spread of 1.4 GeV/c (rms)

are selected by the first two magnets in a four dipole achromat and by momentum-defining slits incorporated into a 3.2 m thick copper/iron proton beam dump, which also blocks the negatively-charged particles. The beam subsequently passes through acceptance-defining and cleaning collimators and a set of four quadrupoles of alternating polarity, as well as muon sweeping magnets, before entering the fiducial decay volume contained in a 114 m long cylindrical vacuum tank with a diameter of 1.92 m upstream, increasing to 2.4 m downstream.

With about 1.8×10^{12} primary protons incident on the target per SPS pulse of about 4.8 s duration repeating every 14.4 or 16.8 s, the secondary beam flux at the entrance of the decay volume is 2.5×10^7 particles per pulse. The fractions of K^+, π^+, p^+, e^+ and μ^+ in the secondary beam are 0.05, 0.63, 0.21, 0.10 and 0.01, respectively. The fraction of those beam kaons decaying in the vacuum tank at nominal momentum is 18%. The beam transverse size at the entrance to the decay volume is $\delta x = \delta y = 4$ mm (rms), and its horizontal and vertical angular divergences are about 20 μrad (rms). The beam central momentum, transverse position at the entrance to the vacuum tank and direction varied slowly over time with respect to the nominal ones in the ranges of ~ 0.1 GeV/c^2, ~ 1 mm and ~ 10 μrad, respectively.

The beam line also transmits certain off-momentum charged kaons and pions punching through the proton beam dump with a suppression factor of $\sim 10^{-3}$. However the subsequent decays of these particles do not contribute to the signal region of the present analysis.

1.2 Detector

The charged particle properties are measured in a magnetic spectrometer, housed in a tank filled with helium at nearly atmospheric pressure, placed after the decay volume and separated from the vacuum by a thin ($\sim 0.4\%$ radiation lengths X_0) Kevlar® window. The spectrometer comprises four drift chambers (DCHs) [12], two upstream and two downstream of a dipole magnet which gives a horizontal transverse momentum kick of 265 MeV/c to singly-charged particles. Each DCH is composed of eight planes of sense wires, and provides a spatial resolution of 90 μm in each projection. The measured momentum resolution is $\sigma_p/p = 0.48\% \oplus 0.009\% \cdot p$, where p is expressed in GeV/c.

A plastic scintillator hodoscope (HOD) producing fast trigger signals and providing precise time measurements of charged particles is placed after the spectrometer. It consists of a plane of vertical strips, followed by a similar plane of horizontal strips (128 counters in total). Both planes have regular octagonal shapes and a central hole for the passage of the beam.

The HOD is followed by a quasi-homogeneous liquid krypton electromagnetic calorimeter (LKr) [13] used for lepton identification and as a photon veto in the present analysis. The LKr is 127 cm (or $27X_0$) thick along the beam, with projective readout consisting of copper/beryllium ribbons extending from the front to the back of the detector. The 13248 readout cells have a transverse size of approximately 2×2 cm^2 each and have no longitudinal segmentation. The energy resolution is $\sigma_E/E = 0.032/\sqrt{E} \oplus 0.09/E \oplus 0.0042$ (E in GeV). The spatial resolution for the transverse coordinates x and y of an isolated electromagnetic shower is $\sigma_x = \sigma_y = 0.42/\sqrt{E} \oplus 0.06$ cm (E in GeV).

An aluminium beam pipe of 158 mm outer diameter and 1.1 mm thickness traversing the centres of all detector elements allows the undecayed beam particles to continue their path in vacuum. The outer transverse sizes of the subdetectors are about 2.4 m.

1.3 Trigger and DAQ

A minimum bias trigger configuration has been employed, resulting in high efficiency. The K_{e2} trigger condition consists of coincidences of signals in the two HOD planes (the Q_1 signal), loose lower and upper limits on DCH hit multiplicity (the 1-track signal), and LKr energy deposit (E_{LKr}) of at least 10 GeV. The $K_{\mu2}$ trigger condition requires a coincidence of the Q_1 and 1-track

signals downscaled by a factor $D = 150$. The non-downscaled $K_{\mu 2}$ trigger rate is 0.5 MHz, and is dominated by beam halo muons; the K_{e2} trigger rate is about 10 kHz. Downscaled control samples based on trigger signals from the DCHs, HOD and LKr have been collected to monitor the performance of the main trigger signals. The data taking took place during four months starting in June 2007. About 40% of the 350k recorded good SPS spills are used for the present analysis.

2 Analysis strategy

The analysis strategy is based on counting the numbers of reconstructed K_{e2} and $K_{\mu 2}$ candidates collected concurrently. Therefore the analysis does not rely on an absolute beam flux measurement, and several systematic effects (due to beam simulation, accidental activity, charged track reconstruction, Q_1 trigger efficiency, and time-dependent effects) cancel at first order.

Due to the significant dependence of acceptance and background on lepton momentum, the R_K measurement is performed independently in 10 momentum bins covering a range from 13 to 65 GeV/c. The lowest momentum bin spans 7 GeV/c, while the others are 5 GeV/c wide. The selection criteria have been optimized separately in each momentum bin. The data samples in the momentum bins are statistically independent, however the systematic errors are partially correlated. The ratio R_K in each bin is computed as

$$R_K = \frac{1}{D} \cdot \frac{N(K_{e2}) - N_{\mathrm{B}}(K_{e2})}{N(K_{\mu 2}) - N_{\mathrm{B}}(K_{\mu 2})} \cdot \frac{A(K_{\mu 2})}{A(K_{e2})} \cdot \frac{f_\mu \times \epsilon(K_{\mu 2})}{f_e \times \epsilon(K_{e2})} \cdot \frac{1}{f_{\mathrm{LKr}}}, \tag{4}$$

where $N(K_{\ell 2})$ are the numbers of selected $K_{\ell 2}$ candidates ($\ell = e, \mu$), $N_{\mathrm{B}}(K_{\ell 2})$ are the numbers of background events, $A(K_{\mu 2})/A(K_{e2})$ is the ratio of the geometric acceptances (referred to as the acceptance correction in the following), f_ℓ are the lepton identification efficiencies, $\epsilon(K_{\ell 2})$ are the trigger efficiencies, f_{LKr} is the global efficiency of the LKr readout (which affects only the K_{e2} selection), and $D = 150$ is the $K_{\mu 2}$ trigger downscaling factor.

To evaluate the acceptance correction and the geometric parts of the acceptances for background processes entering the computation of $N_B(K_{\ell 2})$, a detailed Monte Carlo (MC) simulation based on Geant3 [14] is used. It includes a description, with time variations, of the beam line optics, the full detector geometry, materials, magnetic fields, local inefficiencies of DCH wires, and inactive LKR cells (0.8% of channels). Particle identification, trigger and readout efficiencies are measured directly from data.

3 Data analysis

3.1 Event reconstruction and selection

Charged particle trajectories are reconstructed from hits and drift times in the spectrometer. Track momenta are evaluated using a detailed magnetic field map. Fine calibrations of spectrometer field integral and DCH alignment are performed by monitoring the mean reconstructed $K^+ \to \pi^+ \pi^+ \pi^-$ invariant mass, and the missing mass in $K_{\mu 2}$ decays.

Clusters of energy deposition in the LKr are found by locating the maxima in the digitized pulses from individual cells in both space and time and accumulating the energy within a radius of approximately 11 cm. Shower energies are corrected for energy outside the cluster boundary, energy lost in inactive cells and cluster energy sharing. The energy response has been calibrated with samples of positrons from $K^+ \to \pi^0 e^+ \nu$ decays.

Due to the topological similarity of K_{e2} and $K_{\mu 2}$ decays, a large part of the selection is common for the two decay modes, which leads to significant cancellations of the related systematic uncertainties. The main selection criteria are listed below.

- Exactly one reconstructed charged particle track (lepton candidate) geometrically consistent with originating from a kaon decay is required. The electric charge of the track must be positive.

- The extrapolated track impact points in the DCHs, HOD and LKr must be within their geometrical acceptances. The LKr acceptance condition includes appropriate separations from the detector edges and inactive cells.

- The reconstructed track momentum must be in the range 13 to 65 GeV/c. The lower limit ensures high efficiency of the $E_{\mathrm{LKr}} > 10$ GeV trigger condition. Above the upper limit, the analysis is affected by large uncertainties due to background subtraction.

- No LKr clusters with energy $E > E_{\mathrm{veto}} = 2$ GeV and in time with the track are allowed, unless they can be associated to the track via direct energy deposition or bremsstrahlung. (Most clusters due to bremsstrahlung in front of the spectrometer magnet are resolved from those directly deposited by the track). This requirement provides a photon veto for suppression of backgrounds from $K^+ \to e^+\nu\gamma$, $K^+ \to \pi^0 e^+\nu$, and $K^+ \to \pi^+\pi^0$ decays. However the veto is not hermetic due to the beam pipe and the limited transverse size of the LKr.

- The decay vertex is reconstructed as the point of closest approach of the lepton candidate track extrapolated upstream, and the kaon beam axis. The measured stray magnetic field in the vacuum tank is taken into account. The position of the kaon beam axis is monitored with a sample of fully reconstructed $K^+ \to \pi^+\pi^+\pi^-$ decays.

- The distance from the kaon decay vertex to the beginning of the vacuum tank is required to exceed a minimum value ranging from 8 m at low lepton momentum to 43 m at high momentum, which removes the bulk of the beam halo background (discussed in Section 3.2.4).

- For further suppression of the beam halo and several other backgrounds, the reconstructed closest distance of approach of the track to the beam axis must not exceed 3.5 cm.

The following two main criteria are used to distinguish K_{e2} from $K_{\mu2}$ decays.

- The kinematic identification of K_{e2} ($K_{\mu2}$) decays is based on constraining the reconstructed squared missing mass in the positron (muon) hypothesis:

$$- M_1^2 < M_{\mathrm{miss}}^2(\ell) = (P_K - P_\ell)^2 < M_2^2. \tag{5}$$

Here P_K is the average kaon four-momentum (monitored in time with $K^+ \to \pi^+\pi^+\pi^-$ decays), and P_ℓ is the reconstructed lepton four-momentum (under the positron or muon mass hypothesis). The limits M_1^2 and M_2^2 have been optimized for each lepton momentum bin, taking into account the $M_{\mathrm{miss}}^2(\ell)$ resolution (which varies from 0.0025 (GeV/c^2)^2 at mid track momentum to 0.005 (GeV/c^2)^2 at low and high track momentum), the radiative mass tails, and the background conditions. M_1^2 varies between 0.013 and 0.016 (GeV/c^2)^2 and M_2^2 between 0.010 and 0.013 (GeV/c^2)^2. The kinematic separation of K_{e2} and $K_{\mu2}$ decays is illustrated in Fig. 1a.

- The lepton identification is based on the ratio E/p of energy deposition in the LKr to momentum measured by the spectrometer. Charged particles with $(E/p)_{\mathrm{min}} < E/p < 1.1$, where $(E/p)_{\mathrm{min}} = 0.95$ for $p > 25$ GeV/c and $(E/p)_{\mathrm{min}} = 0.9$ otherwise, are identified as positrons. At low lepton momenta, the background from particle mis-identification is negligible. For $p > 25$ GeV/c, the larger $(E/p)_{\mathrm{min}}$ limit minimises the net uncertainty from
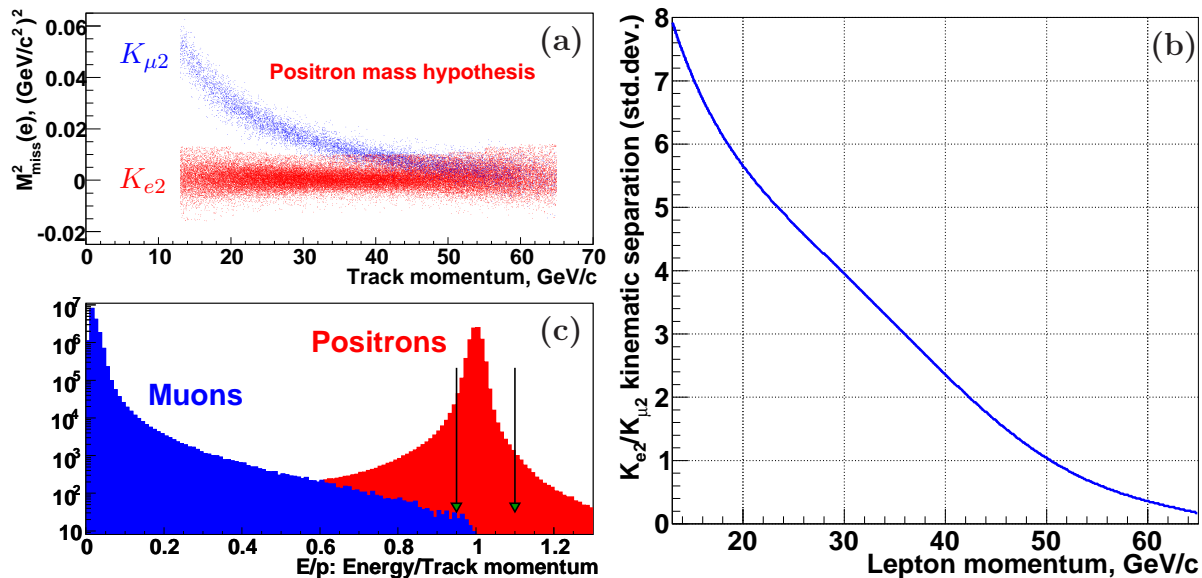
Figure 1: (a) Squared missing mass assuming the positron mass hypothesis $M^2_{\text{miss}}(e)$ as a function of lepton momentum for reconstructed K_{e2} and $K_{\mu 2}$ decays (data); (b) K_{e2} vs $K_{\mu 2}$ kinematic separation (standard deviations) as a function of lepton momentum; (c) E/p spectra of positrons and muons (data); the positron identification limits for $p > 25$ GeV/c are indicated by arrows.

$K_{\mu 2}$ background subtraction and particle mis-identification inefficiency. Charged particles with $E/p < 0.85$ are classified as muons. The data E/p spectra of positrons and muons are shown in Fig. 1c.

3.2   The K_{e2} sample

The number of K_{e2} candidates in the signal region is $N(K_{e2}) = 59813$. The sources of background in the K_{e2} sample are discussed below.

3.2.1 $K_{\mu 2}$ background

Kinematic separation of K_{e2} from $K_{\mu 2}$ decays is achievable at low lepton momentum only ($p \lesssim 35$ GeV/c), as shown in Figs. 1a and 1b. At high lepton momentum, the $K_{\mu 2}$ decay with a mis-identified muon ($E/p > 0.95$, see Fig. 1c) is the largest background source. The dominant process leading to mis-identification of the muon as a positron is 'catastrophic' bremsstrahlung in or in front of the LKr leading to significant energy deposit in the LKr. Mis-identification due to accidental LKr clusters associated with the muon track is negligible, as concluded from a study of the sidebands of track-cluster time difference and distance distributions.

The muon mis-identification probability $P_{\mu e}$ has been measured as a function of momentum. To collect a muon sample free from the typical $\sim 10^{-4}$ positron contamination due to $\mu \to e$ decays, a $9.2X_0$ thick lead (Pb) wall covering $\sim 20\%$ of the geometric acceptance was installed approximately 1.2 m in front of the LKr calorimeter (between the two HOD planes) during a dedicated period of data taking with K^+ and K^- beams. The K_{e2} sample collected with the Pb wall installed is not used for the R_K measurement. The component from positrons which traverse the Pb wall and are mis-identified as muons from $K_{\mu 2}$ decay with $p > 30$ GeV/c and $E/p > 0.95$ is suppressed down to a negligible level ($\sim 10^{-8}$) by energy losses in the Pb.

However, muon passage through the Pb wall affects the measured $P^{\text{Pb}}_{\mu e}$ via two principal effects: 1) ionization energy loss in Pb decreases $P_{\mu e}$ and dominates at low momentum; 2)
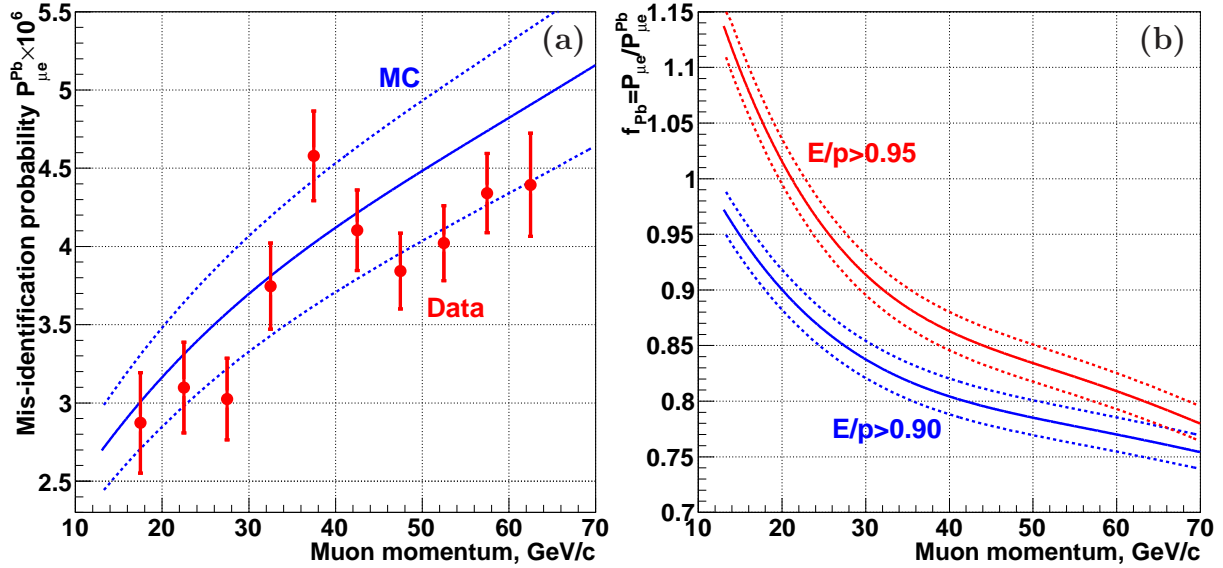
Figure 2: (a) Mis-identification probability for muons traversing the lead wall, $P_{\mu e}^{\mathrm{Pb}}$, for $(E/p)_{\mathrm{min}} = 0.95$ as a function of momentum: measurement (solid circles with error bars) and simulation (solid line). (b) Correction factors $f_{\mathrm{Pb}} = P_{\mu e}/P_{\mu e}^{\mathrm{Pb}}$ for the considered values of $(E/p)_{\mathrm{min}}$, as evaluated with simulation. Dotted lines in both plots indicate the estimated systematic uncertainties of the simulation.

bremsstrahlung in Pb increases $P_{\mu e}$ and dominates at high momentum. To evaluate the correction factor $f_{\mathrm{Pb}} = P_{\mu e}/P_{\mu e}^{\mathrm{Pb}}$, a dedicated MC simulation based on Geant4 (version 9.2) [15] has been developed to describe the propagation of muons downstream from the last DCH, involving all electromagnetic processes including muon bremsstrahlung [16].

The measurements of $P_{\mu e}^{\mathrm{Pb}}$ in momentum bins compared with the results of the MC simulation and the correction factors f_{Pb} obtained from simulation, along with the estimated systematic uncertainties of the simulated values, are shown in Fig. 2. The relative systematic uncertainties on $P_{\mu e}$ and $P_{\mu e}^{\mathrm{Pb}}$ obtained by simulation have been estimated to be 10%, and are mainly due to the simulation of cluster reconstruction and energy calibration. However the error of the ratio $f_{\mathrm{Pb}} = P_{\mu e}/P_{\mu e}^{\mathrm{Pb}}$ is significantly smaller ($\delta f_{\mathrm{Pb}}/f_{\mathrm{Pb}} = 2\%$) due to cancellation of the main systematic effects. The measured $P_{\mu e}^{\mathrm{Pb}}$ is in agreement with the simulation within their uncertainties.

The positive correlation between the reconstructed $M_{\mathrm{miss}}^2(e)$ and E/p, which are both computed using the reconstructed track momentum, leads to an apparent dependence of $P_{\mu e}$ on $M_{\mathrm{miss}}^2(e)$. This effect is significant for intermediate lepton momenta where the $K_{\mu 2}$ background comes from events with underestimated $M_{\mathrm{miss}}^2(e)$ and a smaller muon mis-identification probability (see Fig. 1a). This correlation has been taken into account.

The $K_{\mu 2}$ background contamination integrated over lepton momentum has been computed to be $(6.11 \pm 0.22)\%$ using the measured $P_{\mu e}^{\mathrm{Pb}}$ corrected by f_{Pb}. The quoted error comes from the limited size of the data sample used to measure $P_{\mu e}^{\mathrm{Pb}}$ (0.16%), the uncertainty δf_{Pb} (0.12%), and the model-dependence of the correction for the $M_{\mathrm{miss}}^2(e)$ vs E/p correlation (0.08%). The first error component is uncorrelated between the lepton momentum bins, while the others are fully correlated.

As a stability check, the evaluation of $P_{\mu e}$ has been performed with an additional requirement that the energy deposit in the HOD counters downstream from the Pb wall is small (limited to the equivalent of 1.5 to 3 minimum ionizing particles), which strongly suppresses muons undergoing bremsstrahlung in the Pb wall. The stability of $P_{\mu e}$ is consistent with the assigned uncertainty δf_{Pb}. Additionally, a stability check of R_K with respect to variation of $(E/p)_{\mathrm{min}}$

for lepton momentum $p > 25$ GeV/c in the range from 0.90 to 0.97 has been performed. The observed relative stability of R_K within $\pm 0.2\%$, although the $K_{\mu 2}$ background varies from 17% to 3%, is consistent with the uncertainty assigned to the $K_{\mu 2}$ background.

The $K_{\mu 2}$ decay also contributes to background via $\mu^+ \to e^+ \nu \bar{\nu}$ decays in flight. Energetic forward secondary positrons compatible with K_{e2} kinematics and topology are suppressed by muon polarisation effects [17]. Radiative corrections to the muon decay [18] lead to a further $\sim 10\%$ relative background suppression. This background contamination has been estimated to be $(0.27 \pm 0.04)\%$, where the dominant uncertainty is due to the simulated statistics.

3.2.2 $K^+ \to e^+ \nu \gamma$ background

R_K is defined to be fully inclusive of internal bremsstrahlung (IB) radiation [1]. The structure-dependent (SD) $K^+ \to e^+ \nu \gamma$ process [19, 20] may lead to a K_{e2} signature if the extra photon is undetected. In particular, the SD$^+$ component with positive photon helicity peaks at high positron momentum in the K^+ rest frame ($E_e^* \approx M_K/2$) and has a similar branching ratio to K_{e2}. The background due to $K^+ \to e^+ \nu \gamma$ (SD$^-$) decay with negative photon helicity and the interference between the IB and SD processes are negligible.

The SD$^+$ background contribution has been estimated by MC simulation as $(1.07 \pm 0.05)\%$, using a recent measurement of the $K^+ \to e^+ \nu \gamma$ (SD$^+$) differential decay rate [9]. The quoted uncertainty is due to the limited precision on the form factors and decay rate, and is therefore correlated between lepton momentum bins. A stability check of R_K against variation of the E_{veto} limit in a wide range has been performed. While the $K^+ \to e^+ \nu \gamma$ (SD$^+$) background is enhanced by a factor of 4.5 for $E_{\text{veto}} = 14$ GeV with respect to $E_{\text{veto}} = 2$ GeV, R_K remains stable within $\pm 0.1\%$, which is consistent with the above uncertainty.

3.2.3 $K^+ \to \pi^0 e^+ \nu$ and $K^+ \to \pi^+ \pi^0$ backgrounds

The $K^+ \to \pi^0 e^+ \nu$ decay produces a K_{e2} signature if the only reconstructed particle is an e^+ from K^+ or π^0 Dalitz ($\pi_D^0 \to \gamma e^+ e^-$) decays. The $K^+ \to \pi^+ \pi^0$ decay leads to a K_{e2} signature if the only reconstructed particle is a π^+ mis-identified as e^+, or an e^+ from a $\pi_D^0 \to \gamma e^+ e^-$ decay. The pion mis-identification probability ($0.95 < E/p < 1.1$) has been measured to be $(0.41 \pm 0.02)\%$ in the relevant momentum range from samples of $K^+ \to \pi^+ \pi^0$ and $K_L^0 \to \pi^\pm e^\mp \nu$ decays (the latter collected during a special run).

Kinematically, $K^+ \to \pi^0 e^+ \nu$ and $K^+ \to \pi^+ \pi^0$ decays can be reconstructed with low missing mass in the K_{e2} signal region, either because the charged track undergoes a large multiple scatter or because the kaon is in the high momentum tail of the beam distribution. The systematic uncertainties due to subtraction of these backgrounds have been estimated as 50% of the contributions themselves, due to the limited precision of the simulation of the kaon momentum-distribution tails. The backgrounds are at a level below 0.1%.

3.2.4 Beam halo background

As no tracking is available in the beam region to tag an incoming kaon, beam halo muons can become a source of background to K_{e2} decays in case of $\mu^+ \to e^+ \nu \bar{\nu}$ decay or muon mis-identification as a positron. The choice of the signal region in terms of the longitudinal position of the kaon decay vertex has been dictated by the kinematic distribution of this background (which peaks in the upstream part of the vacuum volume).

The halo background has been measured directly by reconstructing the K_{e2}^+ candidates from one control data sample collected with the K^- beam transmitted by the beam line and the K^+ beam (but not its halo) blocked, and another control data sample collected with both K^+ and K^- beams blocked. The control samples are normalised to the data in the region

Table 1: Summary of backgrounds in the K_{e2} sample.

Source	$N_B/N(K_{e2})$
$K_{\mu 2}$	$(6.11 \pm 0.22)\%$
$K_{\mu 2}(\mu \to e)$	$(0.27 \pm 0.04)\%$
$K^+ \to e^+ \nu \gamma$ (SD$^+$)	$(1.07 \pm 0.05)\%$
$K^+ \to \pi^0 e^+ \nu$	$(0.05 \pm 0.03)\%$
$K^+ \to \pi^+ \pi^0$	$(0.05 \pm 0.03)\%$
Beam halo	$(1.16 \pm 0.06)\%$
Total	$(8.71 \pm 0.24)\%$

$-0.3 < M^2_{\mathrm{miss}}(\mu) < -0.1$ $(\mathrm{GeV}/c^2)^2$ populated mainly by beam halo events. The 'cross-talk' probability to reconstruct a K^+_{e2} candidate due to a K^- decay with e^+ emission ($K^- \to \pi^0_D \ell^- \nu$, $K^- \to \pi^- \pi^0_D$, $K^- \to \ell^- \nu e^+ e^-$ with $\ell = e, \mu$) is at the level of $\sim 10^{-4}$ and is taken into account. The halo background rate and kinematical distribution are qualitatively reproduced by a simulation of the beam line.

The background contamination has been estimated to be $(1.16 \pm 0.06)\%$, where the error comes from the limited size of the control samples (uncorrelated between lepton momentum bins) and the normalisation uncertainty due to decays of beam kaons and pions upstream of the decay volume (correlated between momentum bins).

3.2.5 Summary of backgrounds in the K_{e2} sample

Backgrounds integrated over lepton momentum are summarised in Table 1. The total background contamination is $(8.71 \pm 0.24)\%$; its uncertainty is smaller than the relative statistical uncertainty of 0.43%. The $M^2_{\mathrm{miss}}(e)$ and lepton momentum distributions of K_{e2} candidates and backgrounds are shown in Fig. 3.

3.3 The $K_{\mu 2}$ sample

The number of $K_{\mu 2}$ candidates collected with a trigger chain involving downscaling by a factor of 150 is $N(K_{\mu 2}) = 1.803 \times 10^7$. The only significant background source in the $K_{\mu 2}$ sample is the beam halo. Its contribution is mainly at low muon momentum, and has been measured to be $(0.38 \pm 0.01)\%$ using the same technique as for the K_{e2} sample. The $M^2_{\mathrm{miss}}(\mu)$ and muon momentum spectra of $K_{\mu 2}$ candidates and the halo background are presented in Fig. 4.

3.4 Geometrical acceptance correction

The ratio of geometric acceptances $A(K_{\mu 2})/A(K_{e2})$ in each lepton momentum bin has been evaluated with MC simulation. The radiative $K^+ \to e^+ \nu \gamma$ (IB) process, which is responsible for the loss of about 5% of the K_{e2} acceptance by increasing the reconstructed $M^2_{\mathrm{miss}}(e)$, is taken into account following [19], with higher order corrections according to [21, 22].

The acceptance correction is strongly influenced by bremsstrahlung suffered by the positron in the material upstream of the spectrometer magnet (Kevlar window, helium, DCHs). This results in an almost momentum-independent loss of K_{e2} acceptance of about 6%, mainly by increasing the reconstructed $M^2_{\mathrm{miss}}(e)$. The relevant material thickness has been measured by studying the spectra and rates of bremsstrahlung photons produced by low intensity 25 GeV/c and 40 GeV/c electron and positron beams steered into the DCH acceptance, using special data samples collected in the same setup by the NA48/2 experiment in 2004 and 2006. Using these
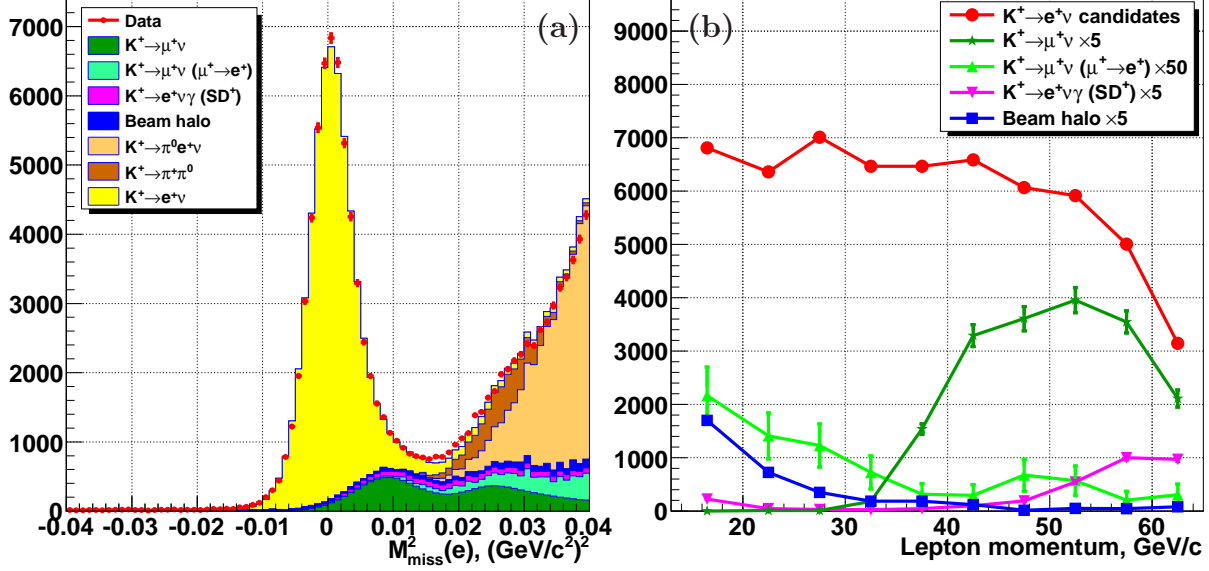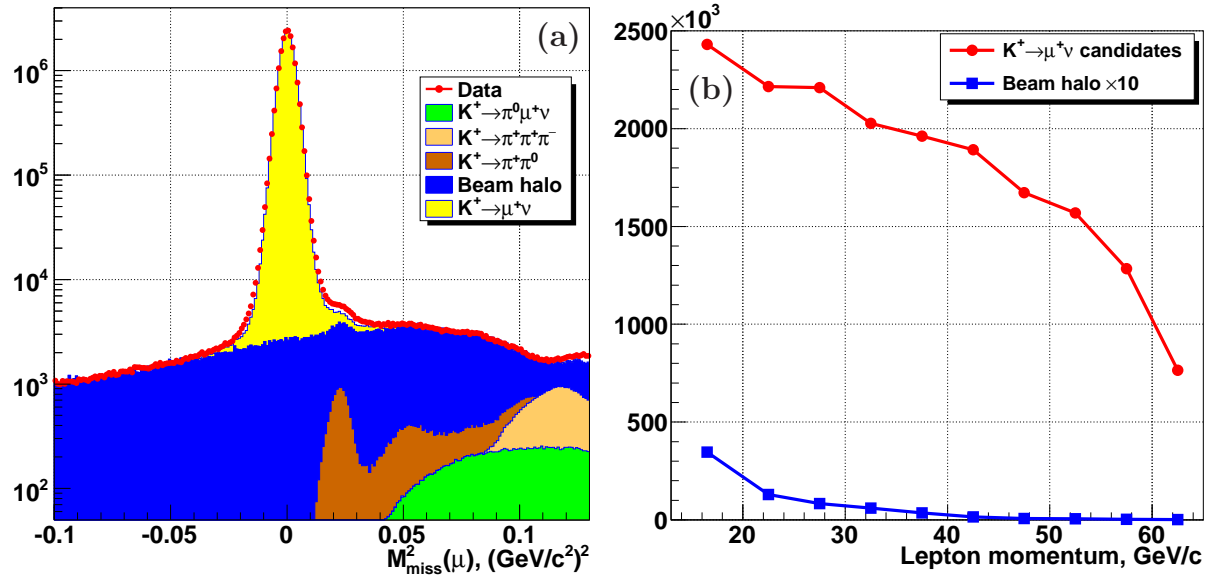
Figure 3: (a) Reconstructed squared missing mass $M^2_{\mathrm{miss}}(e)$ distribution of the K_{e2} candidates compared with the sum of normalised estimated signal and background components. The small discrepancy between data and MC at low $M^2_{\mathrm{miss}}(e)$ is due to the limited precision of MC beam description, which is taken into account by systematic uncertainty due to the acceptance correction. (b) Lepton momentum distributions of the K_{e2} candidates and the dominant backgrounds; the backgrounds are scaled for visibility.

Figure 4: (a) Reconstructed squared missing mass $M^2_{\mathrm{miss}}(\mu)$ distribution of the $K_{\mu2}$ candidates compared with the sum of normalised estimated signal and background components. The deficit of reconstructed MC events in the region of the $K^+ \to \pi^+\pi^0$ peak is due to the limited precision of the beam simulation, and is mostly outside the signal region. (b) Lepton momentum distributions of the $K_{\mu2}$ candidates and the beam halo background (the latter is scaled for visibility).
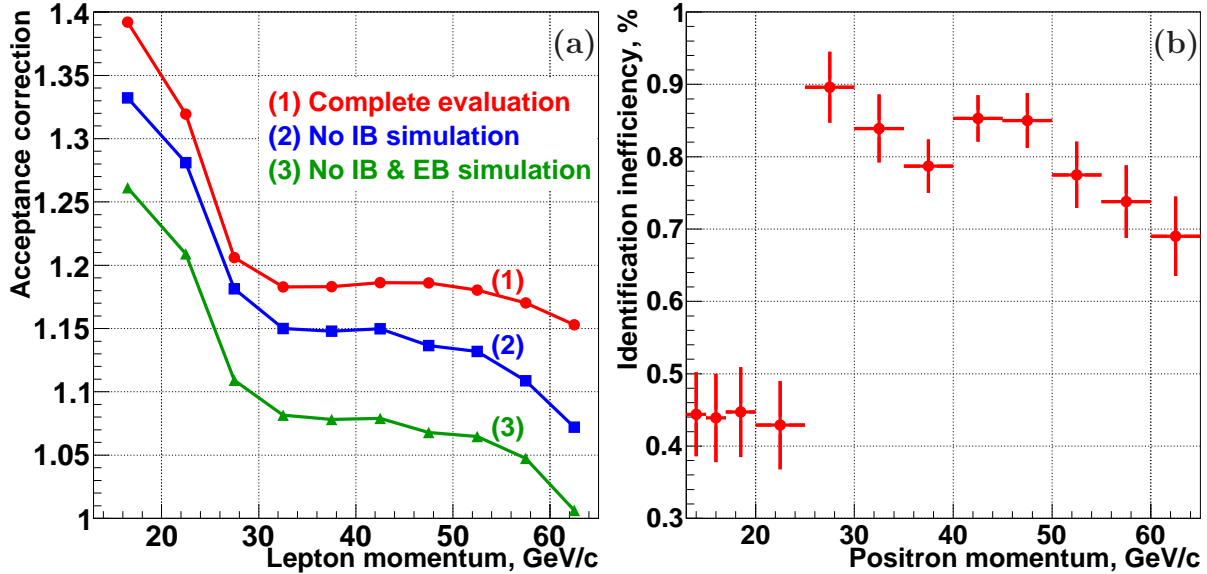
Figure 5: (a) The acceptance correction $A(K_{\mu 2})/A(K_{e2})$ in lepton momentum bins; the corrections neglecting internal (IB) and external (EB) bremsstrahlung radiation are also presented. (b) The measured positron identification inefficiency $1 - f_e$ in lepton momentum bins; uncertainties in bins are partially correlated. The lower inefficiency for $p < 25$ GeV/c is due to the relaxed positron identification requirement discussed in Section 3.1.

measurements, the material thickness during the 2007 run has been estimated to be $(1.56 \pm 0.03)\% X_0$. The quoted uncertainty is dominated by the limited knowledge of helium purity in the spectrometer tank; its measured purity of $(92 \pm 4)\%$ corresponds to a thickness of $(0.26 \pm 0.03)\% X_0$. This translates into a systematic uncertainty on R_K.

The acceptance correction $A(K_{\mu 2})/A(K_{e2})$ in lepton momentum bins is presented in Fig. 5a. The corrections evaluated without internal (IB) and external (EB) bremsstrahlung radiation are also presented to illustrate the magnitudes of the corresponding effects. The correction is enhanced at low lepton momentum because the radial distributions of positrons from K_{e2} decays in the DCH planes are wider than those of muons from $K_{\mu 2}$ decays, and low momentum leptons are not fully contained within the geometric acceptance due to the limited transverse sizes of the DCHs.

The track reconstruction inefficiency due to interactions in spectrometer material is included into the acceptance correction. Simulation of the positron track reconstruction inefficiency (which is $\sim 10^{-3}$ in the analysis track momentum range) has been validated with a sample of $K^+ \to \pi^+ \pi_D^0$ decays. The muon track reconstruction inefficiency evaluated with MC simulation is $\sim 2 \times 10^{-4}$. Systematic effects due to imperfect simulation of the reconstruction efficiency are negligible.

Apart from helium purity, the main sources of systematic uncertainty of the acceptance correction are the limited knowledge of beam profile and divergence, and the simulation of soft radiative photons. A separate uncertainty has been assigned to account for the finite precision of the DCH alignment.

3.5 Lepton identification efficiencies

The E/p ratio provides powerful particle identification criteria. The momentum-dependent positron identification window $(E/p)_{\min} < E/p < 1.1$ includes more than 99% of the K_{e2} events, while suppressing muons by a factor of $1/P_{\mu e} \sim 10^6$. The requirement $E/p < 0.85$ leads

13

to a negligible inefficiency of the muon identification.

A pure sample of 4×10^7 positrons, selected kinematically from $K^+ \to \pi^0 e^+ \nu$ (charged K_{e3}) decays collected with the K_{e2} trigger concurrently with the main $K_{\ell2}$ data set, is used to calibrate the energy response of each LKr cell and to study f_e with respect to local position and time stability. However, the momentum range of the positrons from charged K_{e3} decays is kinematically limited, preventing a sufficiently precise measurement of f_e above 50 GeV/c. Therefore a dedicated data sample was recorded in a special 15 hour long run with a broad momentum band K_L^0 beam. Electrons and positrons from the 4×10^6 collected $K_L^0 \to \pi^\pm e^\mp \nu$ (neutral K_{e3}) decays allow the determination of f_e in the whole analysis momentum range.

The measurements of f_e have been performed in bins of lepton momentum; a finer binning is used inside the lowest of the 10 standard bins to improve the determination of local inefficiencies, which peak at low momentum. Separate measurements have been performed for several identified groups of LKr cells with higher local inefficiencies. Efficiency measurements with the charged and neutral K_{e3} decays agree to better than 0.1%. Fig. 5b shows the measurements of $1 - f_e$ in momentum bins used to evaluate corrections to R_K, obtained as the weighted mean of charged and neutral K_{e3} measurements for momenta up to 50 GeV/c, and as neutral kaon measurements for higher momenta. The inefficiency averaged over the K_{e2} sample is $1 - f_e = (0.73 \pm 0.05)\%$, where the uncertainty takes into account the statistical precision and the small differences between charged and neutral kaon results.

3.6 Trigger and readout efficiencies

The efficiency of the Q_1 trigger condition has been measured using $K_{\mu2}$ events triggered with a control LKr signal. The inefficiency integrated over the $K_{\mu2}$ sample is $(1.4 \pm 0.1)\%$. As a consequence of its geometric uniformity and the similarity of the K_{e2} and $K_{\mu2}$ distributions over the HOD plane, it nearly cancels between the K_{e2} and $K_{\mu2}$ samples, and the residual systematic bias is negligible. The inefficiency of the 1-track condition also largely cancels in the ratio R_K, but is anyway negligible.

Thus the trigger efficiency correction $\epsilon(K_{\mu2})/\epsilon(K_{e2})$ is determined by the efficiency $\epsilon(E_{\mathrm{LKr}})$ of the LKr energy deposit trigger signal $E_{\mathrm{LKr}} > 10$ GeV entering the K_{e2} trigger chain only. The inefficiency $1 - \epsilon(E_{\mathrm{LKr}})$ is only significant in the lowest lepton momentum bin of $(13, 20)$ GeV/c, which is close to the trigger energy threshold and is thus affected by the online energy resolution. A sample of events triggered with a control Q_1 signal passing all K_{e2} selection criteria except the $M_{\mathrm{miss}}^2(e)$ constraint, therefore dominated by K_{e3} events with two lost photons, has been used to measure $1 - \epsilon(E_{\mathrm{LKr}})$ in the lowest momentum bin to be $(0.41 \pm 0.05_{\mathrm{stat.}})\%$. Corrected for the difference of positron distributions in the LKr plane between the K_{e2} sample and the control sample, it translates into $1 - \epsilon(E_{\mathrm{LKr}}) = (0.61 \pm 0.20)\%$ for the K_{e2} sample. The correction and its uncertainty are significant due to the presence of several locally inefficient regions. The resulting uncertainty on R_K is negligible.

Energetic photons not reconstructed in the LKr may initiate showers by interacting in the DCHs or the beam pipe, causing the DCH hit multiplicities to exceed the limits allowed by the 1-track trigger condition. Among the backgrounds, only the $K^+ \to e^+ \nu \gamma$ (SD$^+$) receives a non-negligible correction due to the 1-track inefficiency. The inefficiency for $K^+ \to \pi^0 e^+ \nu$ events with two lost photons has been measured to vary in the range from 0.1 to 0.3 depending on track momentum. The extrapolation of this result to $K^+ \to e^+ \nu \gamma$ (SD$^+$) with one lost photon relies on simulation. The corresponding uncertainty has been propagated into R_K.

The global LKr readout inefficiency, affecting the K_{e2} reconstruction only, has been measured using an independent readout system to be $1 - f_{\mathrm{LKr}} = (0.20 \pm 0.03)\%$, stable in time. This measurement has been cross-checked, with limited precision, by a study of the LKr response in a sample of $\pi_{DD}^0 \to 4e^\pm$ decays reconstructed from spectrometer information only.
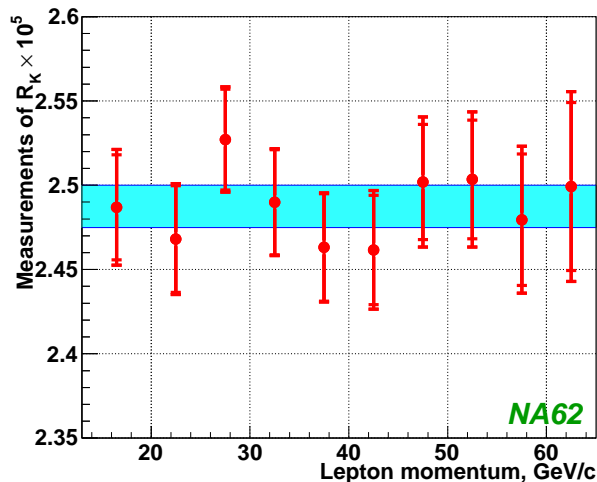
14

Figure 6: Measurements of R_K in lepton momentum bins with their uncorrelated statistical uncertainties and the partially correlated total uncertainties. The average R_K and its total uncertainty are indicated by a band.

Table 2: Summary of the uncertainties on R_K.

Source	$\delta R_K \times 10^5$
Statistical	0.011
$\quad K_{\mu 2}$ background	0.005
$\quad K^+ \to e^+ \nu \gamma$ (SD$^+$) background	0.001
$\quad K^+ \to \pi^0 e^+ \nu$, $K^+ \to \pi^+ \pi^0$ backgrounds	0.001
$\quad$ Beam halo background	0.001
$\quad$ Helium purity	0.003
$\quad$ Acceptance correction	0.002
$\quad$ Spectrometer alignment	0.001
$\quad$ Positron identification efficiency	0.001
$\quad$ 1-track trigger efficiency	0.002
$\quad$ LKr readout inefficiency	0.001
Total systematic	0.007
Total	0.013

4 Result and discussion

A χ^2 fit to the measurements of R_K in the 10 lepton momentum bins has been performed, taking into account the bin-to-bin correlations between the systematic errors. To validate the assigned systematic uncertainties, extensive stability checks have been performed in bins of kinematic variables by varying selection criteria and analysis procedures. The fit result is

$$R_K = (2.487 \pm 0.011_{\text{stat.}} \pm 0.007_{\text{syst.}}) \times 10^{-5} = (2.487 \pm 0.013) \times 10^{-5}, \qquad (6)$$

with $\chi^2/\text{ndf} = 3.6/9$. The individual measurements with their statistical and total uncertainties, and the combined result are displayed in Fig. 6. The uncertainties of the combined result are summarised in Table 2.

This is the most precise R_K measurement to date. It is consistent with the KLOE measurement [9] and the SM expectation $R_K^{\text{SM}} = (2.477 \pm 0.001) \times 10^{-5}$ (Eq. 2), and can be used to set constraints in the space of relevant parameters of multi-Higgs new physics scenarios.

Acknowledgements

References

[1] V. Cirigliano and I. Rosell, Phys. Rev. Lett. **99** (2007) 231801.

[2] A. Masiero, P. Paradisi and R. Petronzio, Phys. Rev. **D74** (2006) 011701.

[3] A. Masiero, P. Paradisi and R. Petronzio, JHEP **0811** (2008) 042.

[4] J. Ellis, S. Lola and M. Raidal, Nucl. Phys. **B812** (2009) 128.

[5] A.G. Clark *et al.*, Phys. Rev. Lett **29** (1972) 1274.

[6] K.S. Heard *et al.*, Phys. Lett. **B55** (1975) 327.

[7] J. Heintze *et al.*, Phys. Lett. **B60** (1976) 302.

[8] K. Nakamura *et al.* (PDG), J. Phys. **G37** (2010) 075021.

[9] F. Ambrosino *et al.*, Eur. Phys. J. **C64** (2009) 627; ibid. **C65** (2010) 703.

[10] V. Fanti *et al.*, Nucl. Instrum. Methods **A574** (2007) 433.

[11] R. Batley *et al.*, Eur. Phys. J. **C52** (2007) 875.

[12] D. Bèderéde *et al.*, Nucl. Instrum. Methods **A367** (1995) 88.

[13] G. Barr *et al.*, Nucl. Instrum. Methods **A370** (1996) 413.

[14] GEANT Description and Simulation Tool, CERN Program Library Long Writeup **W5013** (1994).

[15] S. Agostinelli *et al.*, Nucl. Instrum. Methods **A506** (2003) 250.

[16] S.R. Kelner, R.P. Kokoulin and A.A. Petrukhin, Phys. Atom. Nucl. **60** (1997) 576.

[17] L. Michel, Proc. Phys. Soc. **A63** (1950) 514.

[18] A. Arbuzov, A. Czarnecki and A. Gaponenko, Phys. Rev. **D65** (2002) 113006.

[19] J. Bijnens, G. Ecker and J. Gasser, Nucl. Phys. **B396** (1993) 81.

[20] C.H. Chen, C.Q. Geng and C.C. Lih, Phys. Rev. **D77** (2008) 014004.

[21] S. Weinberg, Phys. Rev. **140** (1965) B516.

[22] C. Gatti, Eur. Phys. J. **C45** (2006) 417.